Submitted to

33rd International Conference on High Energy Physics, ICHEP06, July. 26-Aug.2, 2006, Moscow
Abstract:
Parallel Session **Electroweak**

www-h1.desy.de/h1/www/publications/conf/conf_list.html

Neutral Current Interactions in $e^{\pm}p$ Scattering with Longitudinally Polarised Leptons

H1 Collaboration

Abstract

The inclusive single differential cross section $\mathrm{d}\sigma/\mathrm{d}Q^2$ and the reduced double differential cross section $\tilde{\sigma}(x, Q^2)$ are presented for the neutral current process, $e^{\pm}p \to e^{\pm}X$, in interactions with longitudinally polarised lepton beams. The cross sections are measured in the region of large negative four-momentum transfer squared, $Q^2 \geq 200\,\mathrm{GeV}^2$ and inelasticity, $y < 0.9$. The data are consistent with the expected Q^2 dependence of polarised cross sections, albeit with the limited statistical precision of the data. The reduced cross section data are combined together with previously published unpolarised data to determine the structure function $x\tilde{F}_3$ with improved precision. The data are compared to predictions of the Standard Model which is able to provide a good description of the data.

1 Introduction

HERA measurements of proton structure in neutral current (NC) deep inelastic scattering (DIS) with polarised lepton beams are crucial to the understanding of the detailed dynamics of QCD as well as allowing the chiral structure of electroweak interactions to be simultaneously probed at the highest energies. Previously published measurements [1, 2, 3, 4] have already provided unique constraints [1, 4, 5, 6] on the parton densities functions (PDFs) of the proton as well as the axial and vector couplings of the light quarks to the Z^0 boson [7].

First neutral current (NC) cross section measurements of data taken in the second phase of HERA operation with longitudinally polarised leptons beams have recently been reported [8] for both electron and positron scattering data and are presented here in detail.

In this paper first measurements of the inclusive NC single differential cross sections, $\mathrm{d}\sigma/\mathrm{d}Q^2$ and the reduced cross section $\tilde{\sigma}(x, Q^2)$ are presented for e^+p and e^-p scattering. The data were taken with an incident lepton beam energy of $27.5\,\mathrm{GeV}$, whilst the unpolarised proton beam energy was $920\,\mathrm{GeV}$, yielding a centre-of-mass energy of $\sqrt{s} = 318\,\mathrm{GeV}$. Both data sets are further subdivided into samples of left handed and right handed longitudinal polarisation, $P_e = (N_R - N_L)/(N_R + N_L)$, where N_R (N_L) is the number of right (left) handed leptons in the beam. The corresponding data sets are termed the R and L data sets respectively. The corresponding luminosity and longitudinal lepton beam polarisation is given in Tab. 1 below.

	R	L
e^+p	$\mathcal{L} = 26.9\ \mathrm{pb}^{-1}$ $P_e = (+33.6 \pm 0.6)\%$	$\mathcal{L} = 20.7\ \mathrm{pb}^{-1}$ $P_e = (-40.2 \pm 1.1)\%$
e^-p	$\mathcal{L} = 29.6\ \mathrm{pb}^{-1}$ $P_e = (+37.0 \pm 1.8)\%$	$\mathcal{L} = 68.6\ \mathrm{pb}^{-1}$ $P_e = (-27.0 \pm 1.3)\%$

Table 1: Table of luminosities, $\mathcal{L}$, and luminosity weighted longitudinal polarisation, P_e for the data sets presented here.

2 The Neutral Current Cross Section

The generalised proton structure functions, $\tilde{F}_{2,3}$, may be written as linear combinations of the hadronic structure functions F_2, $F_{2,3}^{\gamma Z}$, and $F_{2,3}^{Z}$ containing information on QCD parton dynamics as well as the EW couplings of the quarks to the neutral vector bosons. The function F_2 is associated to pure photon exchange terms, $F_{2,3}^{\gamma Z}$ correspond to photon-Z^0 interference and $F_{2,3}^{Z}$ correspond to the pure Z^0 exchange terms. In addition the longitudinal structure function $\tilde{F}_L$ may be similarly decomposed, however this is important only at high y and is expected to be negligible at large x (the familiar Bjorken x variable) and Q^2. Neglecting $\tilde{F}_L$, the linear combinations for arbitrarily polarised $e^{\pm}p$ scattering are given by

$$\tilde{F}_2^{\pm} = F_2 - (v_e \pm P_e a_e)\kappa \frac{Q^2}{Q^2 + M_Z^2} F_2^{\gamma Z} + (v_e^2 + a_e^2 \pm P_e 2 v_e a_e)\kappa^2 \left[\frac{Q^2}{Q^2 + M_Z^2}\right]^2 F_2^Z \qquad (1)$$

$$x\tilde{F}_3^{\pm} = -(a_e \pm P_e v_e)\kappa \frac{Q^2}{Q^2 + M_Z^2} x F_3^{\gamma Z} + (2 a_e v_e \pm P_e [v_e^2 + a_e^2])\kappa^2 \left[\frac{Q^2}{Q^2 + M_Z^2}\right]^2 x F_3^Z \qquad (2)$$

Here $\kappa^{-1} = 4\frac{M_W^2}{M_Z^2}(1 - \frac{M_W^2}{M_Z^2})$ in the on-mass-shell scheme [9] with M_W and M_Z the usual weak vector boson masses. For the first time HERA is sensitive to the parity violating terms of the Standard Model, namely those proportional to P_e in eqs. 2 above.

In the quark parton model, the hadronic structure functions are related to linear combinations of sums and differences of the quark and anti-quark momentum distributions $xq(x, Q^2)$ and $x\bar{q}(x, Q^2)$

$$\left[F_2, F_2^{\gamma Z}, F_2^Z\right] = x\sum_q [e_q^2, 2e_q v_q, v_q^2 + a_q^2](q + \bar{q}) \tag{3}$$

$$\left[xF_3^{\gamma Z}, xF3^Z\right] = 2x\sum_q [e_q a_q, v_q a_q](q - \bar{q}) \ , \tag{4}$$

where v_q and a_q are the vector and axial-vector couplings of the light quarks and e_q is the charge of the quark of flavour q.

The differential cross section for $e^\pm$ scattering after correction for QED radiative effects is then given by

$$\frac{\mathrm{d}^2\sigma_{\mathrm{NC}}^\pm}{\mathrm{d}x\mathrm{d}Q^2} = \frac{2\pi\alpha^2}{xQ^4}(Y_+\tilde{F}_2 \mp Y_- x\tilde{F}_3 - y^2\tilde{F}_L) \ , \tag{5}$$

and the reduced cross section is defined by

$$\tilde{\sigma}^\pm(x, Q^2) \equiv \frac{\mathrm{d}^2\sigma_{\mathrm{NC}}^\pm}{\mathrm{d}x\mathrm{d}Q^2}\frac{xQ^4}{2\pi\alpha^2}\frac{1}{Y_+} \equiv \tilde{F}_2 \mp \frac{Y_-}{Y_+}x\tilde{F}_3 - \frac{y^2}{Y_+}\tilde{F}_L \ . \tag{6}$$

The helicity dependence of the electroweak interactions is contained within the terms $Y_\pm = 1 \pm (1 - y^2)$ where y characterises the inelasticity of the interaction.

3 Experimental Technique

The H1 detector components most relevant to this analysis are the liquid argon (LAr) calorimeter, which measures the positions and energies of charged and neutral particles over the polar[1] angular range $4^\circ < \theta < 154^\circ$, and the inner tracking detectors, which measure the angles and momenta of charged particles over the range $7^\circ < \theta < 165^\circ$. A full description of the detector can be found in [10].

The ep luminosity is determined by measuring the QED bremsstrahlung ($ep \to ep\gamma$) event rate by tagging the low angle scattered lepton in a detector located at $z = -44$m adjacent to the beam pipe.

At HERA transverse polarisation of the lepton beam arises naturally through synchrotron radiation via the Sokolov-Ternov effect [11]. In 2000 a pair of spin rotators was installed in the beamline on either side of the H1 detector, allowing transversely polarised leptons to be rotated into longitudinally polarised states and back again. The degree of polarisation is constant around the HERA ring and is continuously measured using two independent polarimeters

[1]The polar angle θ is defined with respect to the positive z axis, the direction of the incident proton beam.

LPOL [12] and TPOL [13]. The polarimeters are situated in beamline sections in which the beam leptons have longitudinal and transverse polarisations respectively. Both measurements rely on an asymmetry in the energy spectrum of left and right handed circularly polarised photons undergoing Compton scattering with the lepton beam. The TPOL measurement uses in addition a spatial asymmetry. The LPOL polarimeter measurements are used when available and TPOL measurements otherwise. The polarisation profile weighted by the luminosity values is shown in Fig. 1(a) and (b) for the e^+ and e^- samples respectively.

Simulated DIS events are used in order to determine acceptance corrections. DIS processes are generated using the DJANGO [14] Monte Carlo (MC) simulation program, which is based on LEPTO [15] for the hard interaction and HERACLES [16] for single photon emission and virtual EW corrections. LEPTO combines $\mathcal{O}(\alpha_s)$ matrix elements with higher order QCD effects using the colour dipole model as implemented in ARIADNE [17]. The JETSET program [18] is used to simulate the hadronisation process. In the event generation the DIS cross section is calculated using the H1 PDF 2000 [4] parametrisation for the proton PDFs.

The dominant ep background contribution arises from photoproduction processes. These are simulated using the PYTHIA [19] MC with leading order PDFs for the proton taken from CTEQ [20] and for the photon from GRV [21]. Further backgrounds from NC DIS, QED-Compton scattering, lepton pair production, prompt photon production and heavy gauge boson ($W^{\pm}$, Z^0) production are also simulated; their final contribution to the analysis sample is small. Further details are given in [4].

The detector response to events produced by the generation programs is simulated in detail using a program based on GEANT [22]. These simulated events are then subjected to the same reconstruction and analysis chain as the data.

The selection of candidate NC events follows closely that of the previously published analysis of unpolarised data from H1 [4] and is briefly described below.

NC events are characterised by an isolated high transverse momentum lepton and a hadronic system opposite in azimuth to the scattered lepton. Such events are triggered mainly using information from the LAr calorimeter. The calorimeter has finely segmented geometry allowing the selection of localised energy deposits in the electromagnetic sections of the calorimeter. This selection is found to be 100% efficient for leptons above 11 GeV.

The hadronic final state particles are reconstructed using a combination of tracks and calorimeter deposits in an energy flow algorithm that avoids double counting [23, 24].

The NC sample is used to carry out an *in-situ* calibration of the electromagnetic and hadronic energy scales of the LAr calorimeter using the method described in [4, 23, 24]. The hadronic calibration procedure is based on the double angle reconstruction method [25] which uses the polar angles of the scattered lepton and the hadronic final state to determine their respective energies. The calibration procedure gives good agreement between data and simulation within an estimated uncertainty of 2% on the hadronic scale and between $1-3\%$ on the electromagnetic scale.

The NC kinematic quantities are determined using the $e\Sigma$ method [26] which uses information from the scattered lepton and the hadronic final state optimising kinematic resolution and minimising QED radiative corrections across the measured kinematic plane.

4 Measurement Procedure

Candidate NC interactions are selected by requiring the scattered lepton energy $E'_e > 11\,\mathrm{GeV}$, $Q^2_e > 133$ GeV^2 and a reconstructed vertex within $35\,\mathrm{cm}$ in z of the nominal interaction point. Background from misidentified leptons is suppressed by requiring a charged track to be associated to the lepton candidate. Longitudinal energy-momentum conservation requires that $E - P_z = 2E_e$ where E_e is the lepton beam energy and E and P_z are the usual components of the hadronic final state four-vector. By requiring $E - P_z > 35$ GeV the influence of radiative corrections is considerably reduced which arises from initial state bremmsstrahlung. This requirement further suppresses the contamination from photoproduction background in which the the scattered lepton is undetected in the backward beam pipe and a hadron is misidentified as a lepton candidate.

The comparison of the data and the simulation (normalised to the luminosity of the data) is shown in Fig. 2 for the distribution of scattered lepton energy E'_e, the lepton polar angle θ_e, the reconstructed Q^2_e, and the transverse momentum balance between the lepton and the hadronic final state, P^h_T/P^e_T. In all cases the simulation provides an accurate description of the data and is used to correct for selection and resolution effects.

The systematic uncertainties on the cross section measurements are discussed briefly below (see [23, 24] and references therein for more details). Positive and negative variations of one standard deviation of each error source are found to yield errors which are symmetric to a good approximation. The systematic uncertainties of each source are taken to be fully uncorrelated between the cross section measurements unless stated otherwise.

- An uncertainty of 1% ($z_{imp} < +20\mathrm{cm}$), 2% ($+20\mathrm{cm} < z_{imp} < +100\mathrm{cm}$) and 3% for $z_{imp} > +100\mathrm{cm}$) is assigned to the scale of the electromagnetic energy measured in the LAr calorimeter, where z_{imp} is the z co-ordinate of the impact position of the scattered lepton in the LAr calorimeter. 1% of this uncertainty is considered as a correlated component.

- An uncertainty of 0.5% for $\theta_e < 100^\circ$ and 2% for $\theta_e > 100^\circ$ in the identification of the scattered electron or positron.

- An uncertainty in the polar angle measurement of the scattered lepton is taken to be 3 mrad.

- An uncertainty of 2% is assigned to the scale of the hadronic energy measured in the detector, of which 1% is considered as a correlated component to the uncertainty.

- A 10% correlated uncertainty is assigned to the amount of energy in the LAr calorimeter attributed to noise.

- A 1% uncertainty on the trigger efficiency.

- A 30% correlated uncertainty on the subtracted ep background is determined from a comparison of data and simulation after relaxing the anti-photoproduction cuts, such that the sample is dominated by photoproduction events.

- The combined uncertainty of finding an interaction vertex and associating a track to the scattered lepton is estimated to be 3% for the e^+p data and 2% for the e^-p data uncorrelated from point to point.
- An uncertainty of 0.5% accounts for the dependence of the acceptance correction on the PDFs used in the MC simulation.
- An error of 1% is estimated for the QED radiative corrections. This accounts for missing contributions in the simulation of the lowest order QED effects and for the uncertainty on the higher order QED and EW corrections.
- An uncertainty of z dependence of the proton bunch structure is estimated to be 0.5%.
- For the e^+p data the relative uncertainty in the measurement of the lepton beam polarisation is taken to be 1.6% for the LPOL and 3.5% for the TPOL [27], yielding a total relative polarisation uncertainty of 1.8% for the R data set and 2.7% for the L data set. For the e^-p data a global relative uncertainty of 5% is considered. These uncertainties are not included in the error bars of the data points.
- In addition, there is a global uncertainty of 2% on the luminosity measurement for both the R and L e^-p data samples, and 1.3% for both e^+p data samples. A correlated component of this uncertainty is estimated to be 0.5%.

The total systematic error is formed by adding the individual uncertainties in quadrature.

5 Results

The measured cross sections $\frac{\mathrm{d}\sigma}{\mathrm{d}Q^2}$ for $y < 0.9$ are shown in Figs. 3 and 4 for e^+p and e^-p scattering respectively. The data are measured in the range $Q^2 \geq 200$ GeV^2 up to $Q^2 \simeq 20\,000$ GeV^2 over which the cross sections fall by almost six orders of magnitude with increasing Q^2. The cross sections are found to be similar at low Q^2 for both lepton charges and polarisations, however at the highest Q^2 differences are observed between the e^+p and e^-p cross sections arising from the structure function $x\tilde{F}_3$.

The measured data are compared to the Standard Model expectation from the H1 PDF 2000 fit [4] which provides an excellent description of the Q^2 dependence of the data including the difference between the e^+p and e^-p cross sections.

The Standard Model also predicts a difference in the cross section for leptons with different helicity states arising from the chiral structure of the neutral electroweak exchange. In Fig. 5 the ratio of cross sections for right polarised to left polarised lepton beams is shown separately for e^+p and e^-p scattering data. In both cases the ratio is found to be consistent, within experimental uncertainty, with unity at low Q^2, indicating little dependence of the cross section on beam polarisation. Note the normalisation uncertainties of the measurements are not included in the errors bars, but are indicated by the dashed lines on the figure. At higher Q^2 the data have a tendency to deviate from unity. For positron scattering the data indicate that right handed

positrons yield a larger cross section than left handed positrons, whereas for electron scattering the data indicate the opposite behaviour. This behaviour is consistent with the Standard Model expectation shown as the solid curve in Fig. 5.

The influence of lepton beam polarisation on the measured cross sections can be enhanced by combining the e^+p and e^-p scattering data in the ratio R defined as

$$\mathrm{R} = \frac{\mathrm{d}\sigma/\mathrm{d}Q^2(e^+p, P_e > 0) + \mathrm{d}\sigma/\mathrm{d}Q^2(e^-p, P_e < 0)}{\mathrm{d}\sigma/\mathrm{d}Q^2(e^+p, P_e < 0) + \mathrm{d}\sigma/\mathrm{d}Q^2(e^-p, P_e > 0)} \quad . \tag{7}$$

For fixed polarisation and at fixed x and Q^2 this is approximately given by

$$\mathrm{R} \simeq \frac{F_2 - P_e a_e \kappa \frac{Q^2}{Q^2+M_Z^2} F_2^{\gamma Z}}{F_2 - P_e a_e \kappa \frac{Q^2}{Q^2+M_Z^2} F_2^{\gamma Z}} \quad , \tag{8}$$

The ratio R is shown in Fig. 6. At low Q^2 R is found to be consistent with unity and deviations from this behaviour are observed with increasing Q^2. The data are consistent with the Standard Model expectation shown as the solid curve albeit within the moderate precision of this data.

The NC polarised data maybe combined into an effective unpolarised e^+p data set and an effective unpolarised e^-p data set after correcting for the small residual polarisations. The unpolarised reduced cross sections are shown for $e^\pm p$ scattering in Fig. 7(a) and demonstrate a clear suppression of the e^+p cross section with respect to the e^-p data. The data compare well to the Standard Model prediction from the H1 PDF 2000 fit in which the observed difference arises from the generalised structure function $x\tilde{F}_3$ (see eq. 6). Thus $x\tilde{F}_3$ may be obtained from

$$x\tilde{F}_3 = \frac{Y_+}{2Y_-}\left[\tilde{\sigma}^-(x,Q^2) - \tilde{\sigma}^+(x,Q^2)\right] \quad . \tag{9}$$

In order to improve the statistical precision the cross section data presented here are combined with the previously published [4] unpolarised NC reduced cross sections in order to determine $x\tilde{F}_3$. The combined HERA-I and HERA-II data are shown in Fig. 7(b) for the region of x and Q^2 where the expected sensitivity is larger than the normalisation uncertainty of the data. In the context of the Standard Model it can be seen from eq. 2 that the dominant contribution to $x\tilde{F}_3$ arises from the γZ interference term, since the pure Z exchange term is suppresed by an additional factor of $\kappa Q^2/(Q^2 + M_Z^2)$ and, in the case of unpolarised scattering, the small vector coupling v_e. Thus $x\tilde{F}_3^{\gamma Z}$ may be determined by

$$xF_3^{\gamma Z} \simeq x\tilde{F}_3 \frac{(Q^2 + M_Z^2)}{a_e \kappa Q^2} \tag{10}$$

neglecting terms proportional to v_e. The data are shown in Fig. 8(a) for three Q^2 values and compared to the expectation. The weak Q^2 dependence of this non-singlet structure function is also shown from the H1 PDF 2000 fit. Since the dependence is weak, the data are transformed to one Q^2 value at $1\,500$ GeV^2 and then averaged. The combination of extracted $xF_3^{\gamma Z}$ data for all Q^2 values is shown in Fig. 8(b) and is directly sensitive to the valence quark distributions. The Standard Model prediction is also shown and found to be in excellent agreement in both shape and magnitude with the data.

In leading order QCD a sum rule [28] predicts that

$$\int_0^1 x F_3^{\gamma Z} \frac{dx}{x} = \frac{1}{3} \int_0^1 (2u_v + d_v) dx = \frac{5}{3}. \tag{11}$$

Higher order corrections to this are expected to be of order α_S/π. The structure function is measured over the x range 0.02 to 0.65 and the integral of $F_3^{\gamma Z}$ is measured to be

$$\int_{0.02}^{0.65} F_3^{\gamma Z} dx = 1.31 \pm 0.15(stat) \pm 0.11(syst) \tag{12}$$

which is consistent with the results of the H1 PDF 2000 fit, 1.12 ± 0.02 and for the same x interval at $Q^2 = 1500\,\mathrm{GeV}^2$.

6 Summary

The NC cross sections $\mathrm{d}\sigma/\mathrm{d}Q^2$ have been measured for $e^{\pm}p$ scattering with longitudinally polarised lepton beams at HERA for the first time. The data are consistent with the predicted behaviour of the polarised ep scattering in the Standard Model with the current limited statistical precision of the measurements.

The double differential NC cross sections $\tilde{\sigma}^{\pm}(x, Q^2)$ have been measured at high Q^2 and an extraction of the structure functions $x\tilde{F}_3$ and $xF_3^{\gamma Z}$ has been performed. The data are in good agreement with expectation of the Standard Model.

Acknowledgements

We are grateful to the HERA machine group whose outstanding efforts have made this experiment possible. We thank the engineers and technicians for their work in constructing and maintaining the H1 detector, our funding agencies for financial support, the DESY technical staff for continual assistance and the DESY directorate for support and for the hospitality which they extend to the non DESY members of the collaboration.

References

[1] C. Adloff *et al.* [H1 Collaboration], Eur. Phys. J. C **21** (2001) 33 [hep-ex/0012053].

[2] C. Adloff *et al.* [H1 Collaboration], Eur. Phys. J. C **13**, 609 (2000) [arXiv:hep-ex/9908059].

[3] C. Adloff *et al.* [H1 Collaboration], Eur. Phys. J. C **19**, 269 (2001) [arXiv:hep-ex/0012052].

[4] C. Adloff *et al.* [H1 Collaboration], Eur. Phys. J. C **30** (2003) 1 [hep-ex/0304003].

[5] D. Stump, J. Huston, J. Pumplin, W.K. Tung, H.L. Lai, S. Kuhlmann and J.F. Owens, JHEP **0310** (2003) 046 [arXiv:hep-ph/0303013].

[6] A.D. Martin, R. G. Roberts, W. J. Stirling and R. S. Thorne, Phys. Lett. B **604** (2004) 61 [arXiv:hep-ph/0410230].

[7] A. Aktas *et al.* [H1 Collaboration], Phys. Lett. B **632** (2006) 35 [hep-ex/0507080].

[8] A. Nikiforov, "Neutral Current in polarised $e^{\pm}p$ collisions at HERA-II", presented on behalf of the H1 Collaboration at XIVth International Workshop on Deep Inelastic Scattering, Tsukuba, Japan, April 2006

[9] A. Sirlin, Phys. Rev. D **22**, 971 (1980).; A. Sirlin, Phys. Rev. D **29**, 89 (1984).

[10] I. Abt *et al.* [H1 Collaboration], Nucl. Instrum. Meth. A **386** (1997) 310 and 348;
R.D. Appuhn *et al.* [H1 SPACAL Group], Nucl. Instrum. Meth. A **386** (1997) 397.

[11] A.A. Sokolov and I.M. Ternov, Sov. Phys. Dokl. **8** No. 12 (1964) 1203.

[12] M. Beckmann *et al.*, Nucl. Instrum. Meth. A **479** (2002) 334.

[13] D.P. Barber *et al.*, Nucl. Instrum. Meth. A **329** (1993) 79.

[14] G.A. Schuler and H. Spiesberger, Proceedings of the Workshop "Physics at HERA", vol. 3, eds. W. Buchmüller, G. Ingelman, DESY (1992) 1419.

[15] G. Ingelman, Proceedings of the Workshop "Physics at HERA", vol. 3,
eds. W. Buchmüller, G. Ingelman, DESY (1992) 1366.

[16] A. Kwiatkowski, H. Spiesberger and H.-J. Möhring, Comput. Phys. Commun. **69** (1992) 155.

[17] L. Lönnblad, Comput. Phys. Commun. **71** (1992) 15.

[18] T. Sjöstrand and M. Bengtsson, Comput. Phys. Commun. **43** (1987) 367.

[19] T. Sjöstrand, Comput. Phys. Commun. **82** (1994) 74.

[20] H.L. Lai *et al.* [CTEQ Collaboration], Eur. Phys. J. C **12** (2000) 375 [hep-ph/9903282].

[21] M. Glück, E. Reya and A. Vogt, Phys. Rev. D **46** (1992) 1973.

[22] R. Brun *et al.*, GEANT3 User's Guide, CERN-DD/EE-84-1 (1987).

[23] B. Portheault, Ph.D. thesis (March 2005), LAL 05-05 (IN2P3/CNRS), Université de Paris-Sud XI, Orsay, available at http://www-h1.desy.de/publications/theses_list.html.

[24] A. Nikiforov, Ph.D. thesis (*in preparation)*, Max-Planck-Institut für Physik, Munich, will be available at http://www-h1.desy.de/publications/theses_list.html.

[25] S. Bentvelsen et.al., Prceedings of the Workshop "Physics at HERA", vol.1, eds. W. Buchmüller, G. Ingelman, DESY (1992) 23; C. Hoeger, ibid, 43.

[26] U. Bassler and G. Bernardi, Nucl. Instrum. Meth. A **361** (1995) 197 [arXiv:hep-ex/9412004]. U. Bassler and G. Bernardi, Nucl. Instrum. Meth. A **426** (1999) 583 [arXiv:hep-ex/9801017].

[27] W. Lorenzon [HERMES Collaboration], DESY-HERMES-97-68, *7th International Workshop on Polarized Gas Targets and Polarized Beams*, Urbana, IL, 18-22 Aug 1997;
F. Corriveau *et al.* [TPOL Polarimeter Group], "A Calibration of the HERA Transverse Polarimeter for the 2003/2004 Data", available at http://www.desy.de/∼pol2000/documents/documents.html.

[28] E. Rizvi and T. Sloan, Eur.Phys.J.C direct, **3** (2001) N2 [hep-ex/0101007].

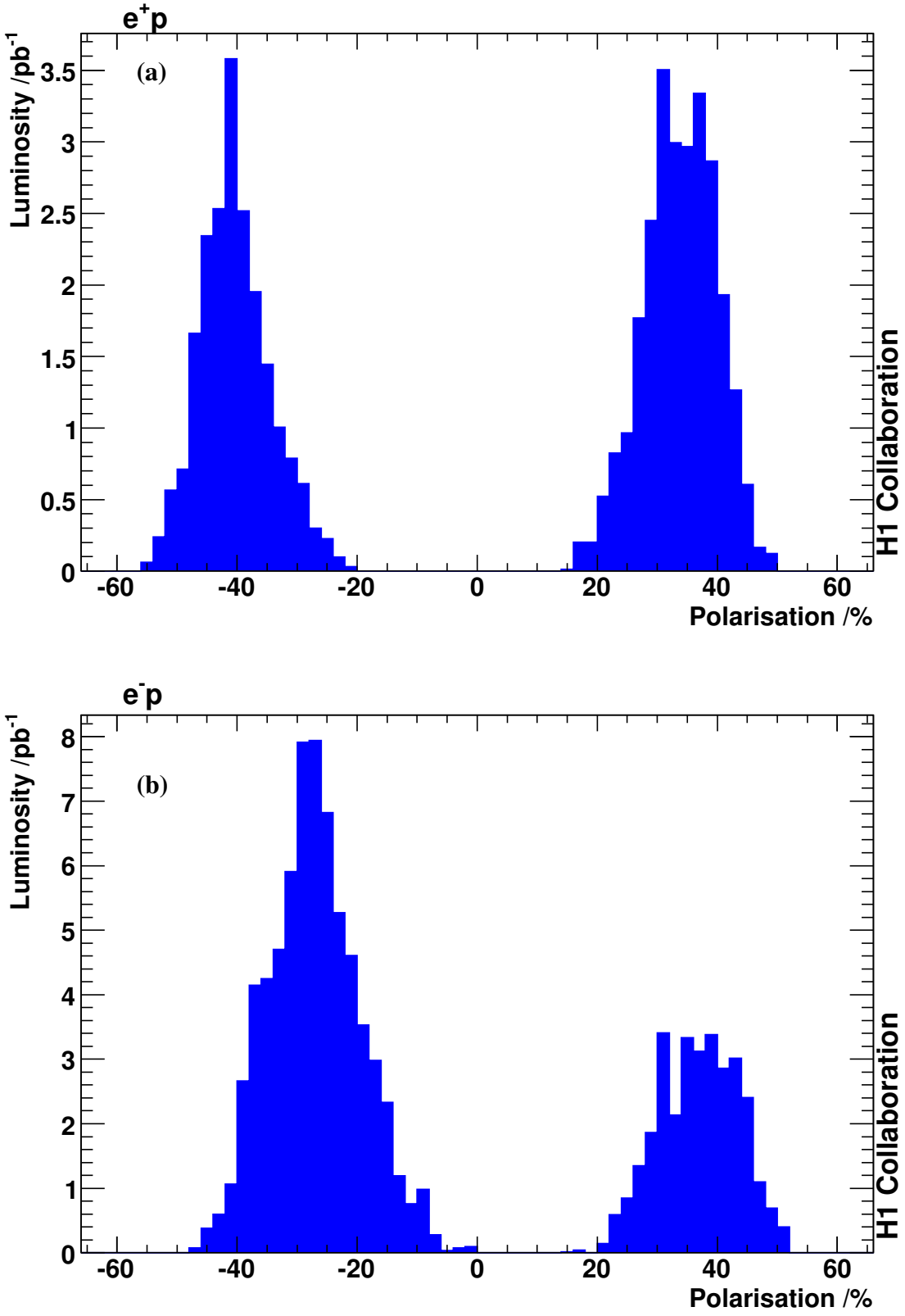

Figure 1: The polarisation profile weighted by the luminosity values for the (a) e^+p data and (b) e^-p data. The $L(R)$ sample corresponds to distribution having negative (positive) polarisation values.

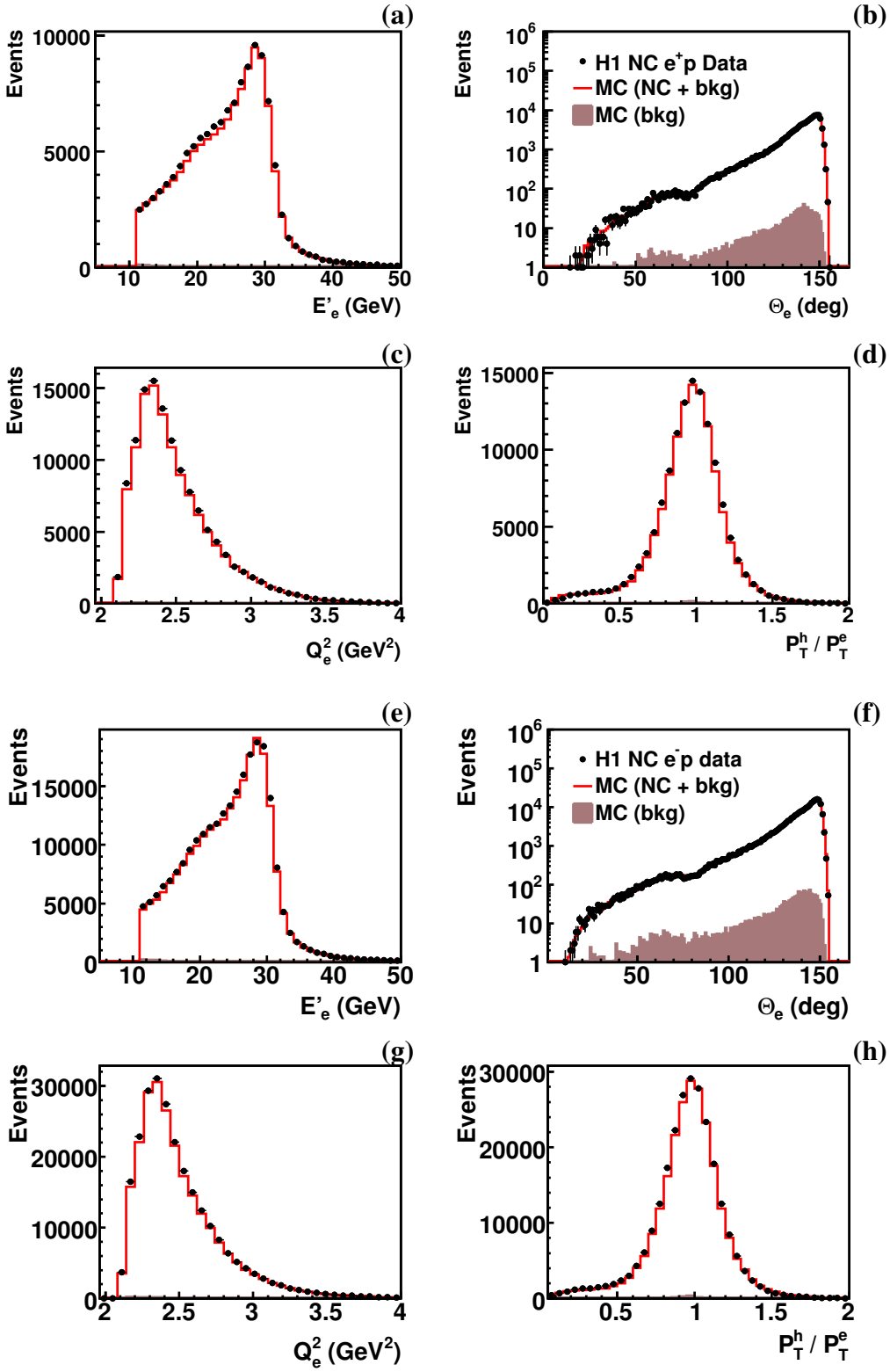

Figure 2: Distributions of (a,e) E'_e, (b,f) θ_e, (c,g) Q^2_e and (d,h) $P_{T,h}/P_{T,e}$ shown in upper and lower plots for the selected events in the (a-d) e^+p and (e-h) e^-p data sets. The Monte Carlo (MC) contributions from the neutral current (NC) process and the ep background (bkg) processes are shown as open histograms with the latter contribution alone being shown as shaded histograms.

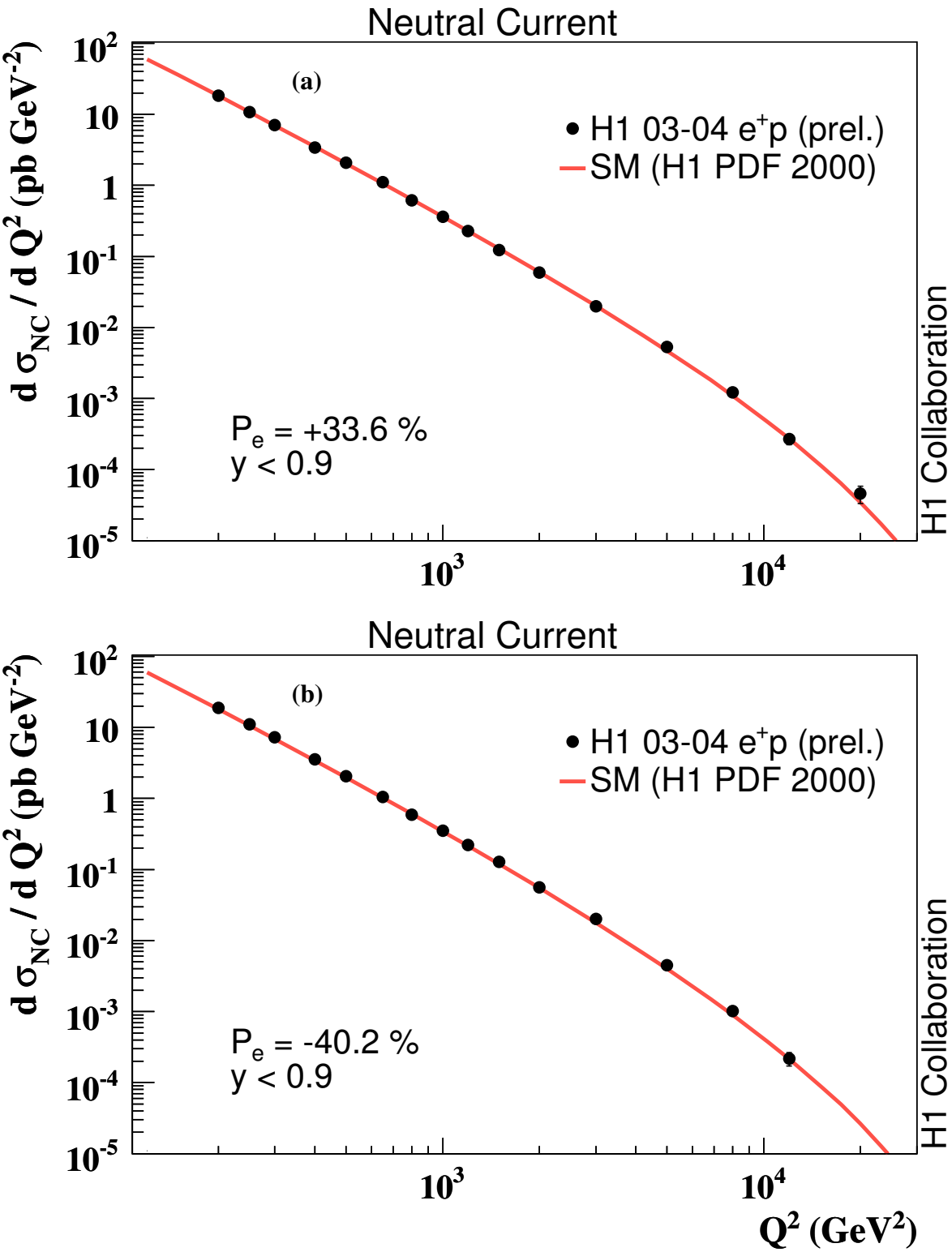

Figure 3: The Q^2 dependence of the NC cross section $\mathrm{d}\sigma/\mathrm{d}Q^2$ for e^+p scattering with the (a) right handed (R) and (b) left handed (L) polarisation data sets. The data (solid points) are compared to the Standard Model prediction.

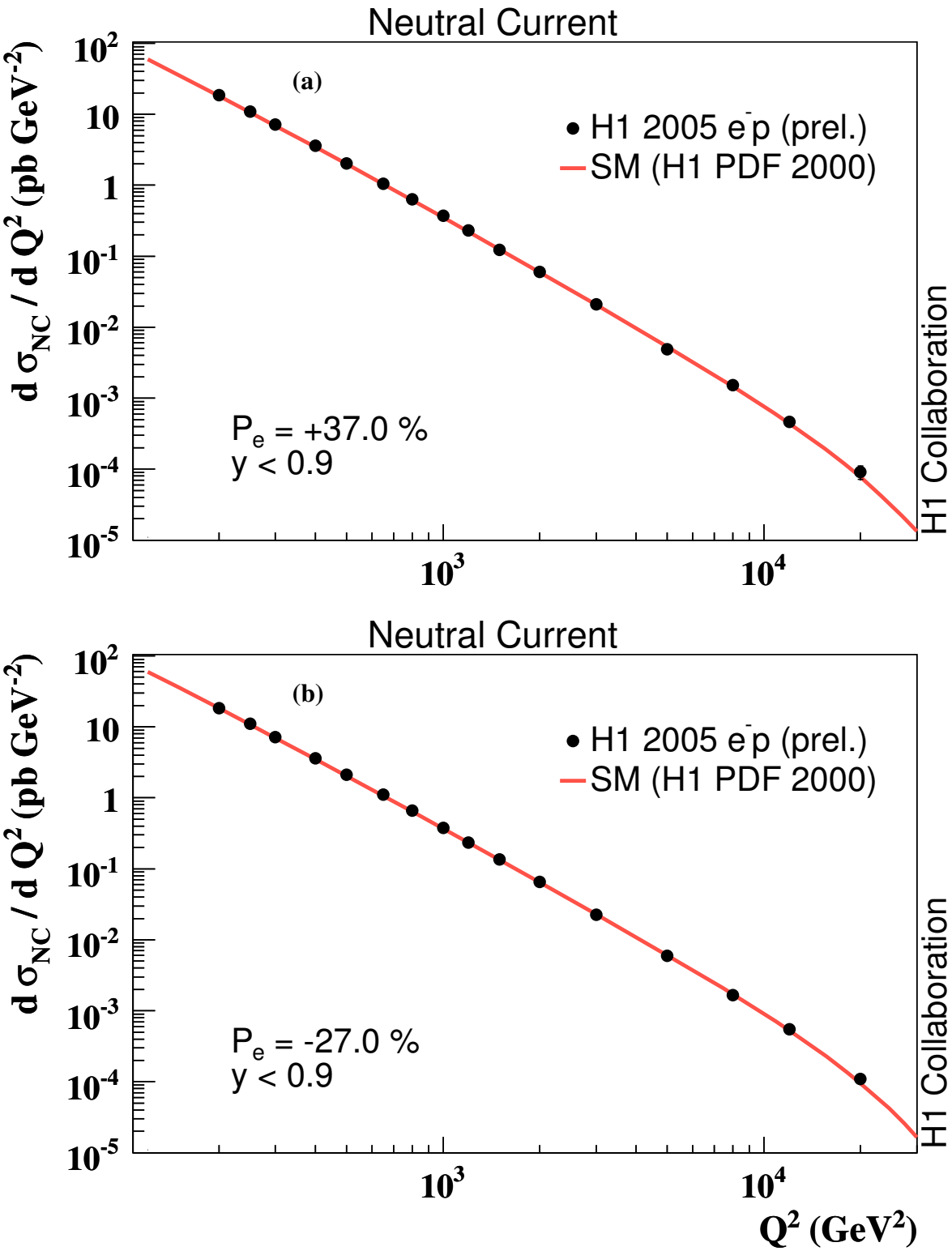

Figure 4: The Q^2 dependence of the NC cross section $\mathrm{d}\sigma/\mathrm{d}Q^2$ for e^-p scattering with the (a) right handed (R) and (b) left handed (L) polarisation data sets. The data (solid points) are compared to the Standard Model prediction.

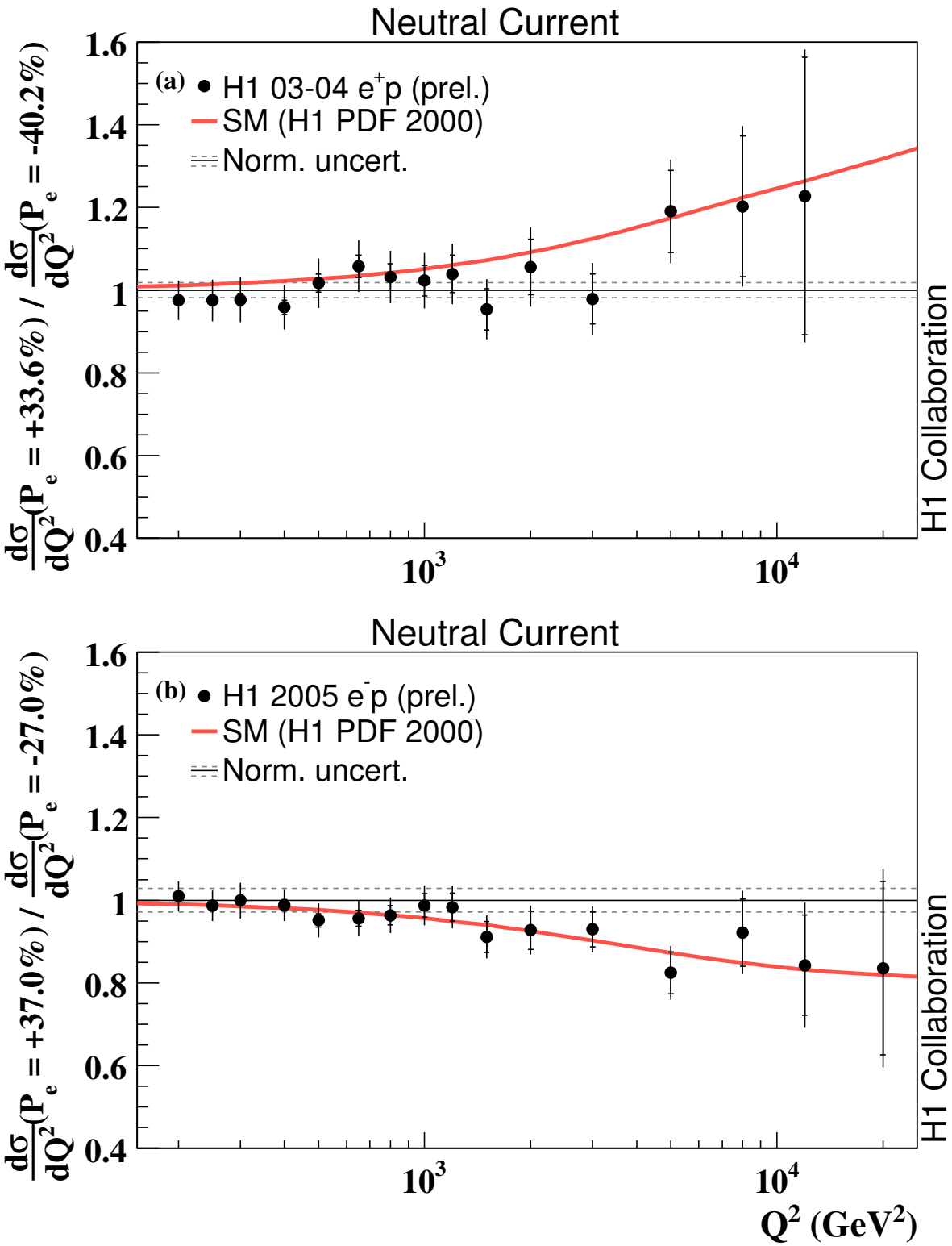

Figure 5: The Q^2 dependences of the NC cross section ratio $\mathrm{d}\sigma/\mathrm{d}Q^2$ R/L for the (a) e^+p scattering and (b) e^-p scattering. The data (solid points) are compared to the Standard Model prediction (solid curve). The inner error bars represent the statistical uncertainties and the outer error bars represent the total errors. The normalisation uncertainty is not included in the error bars and is instead shown as the dashed lines.

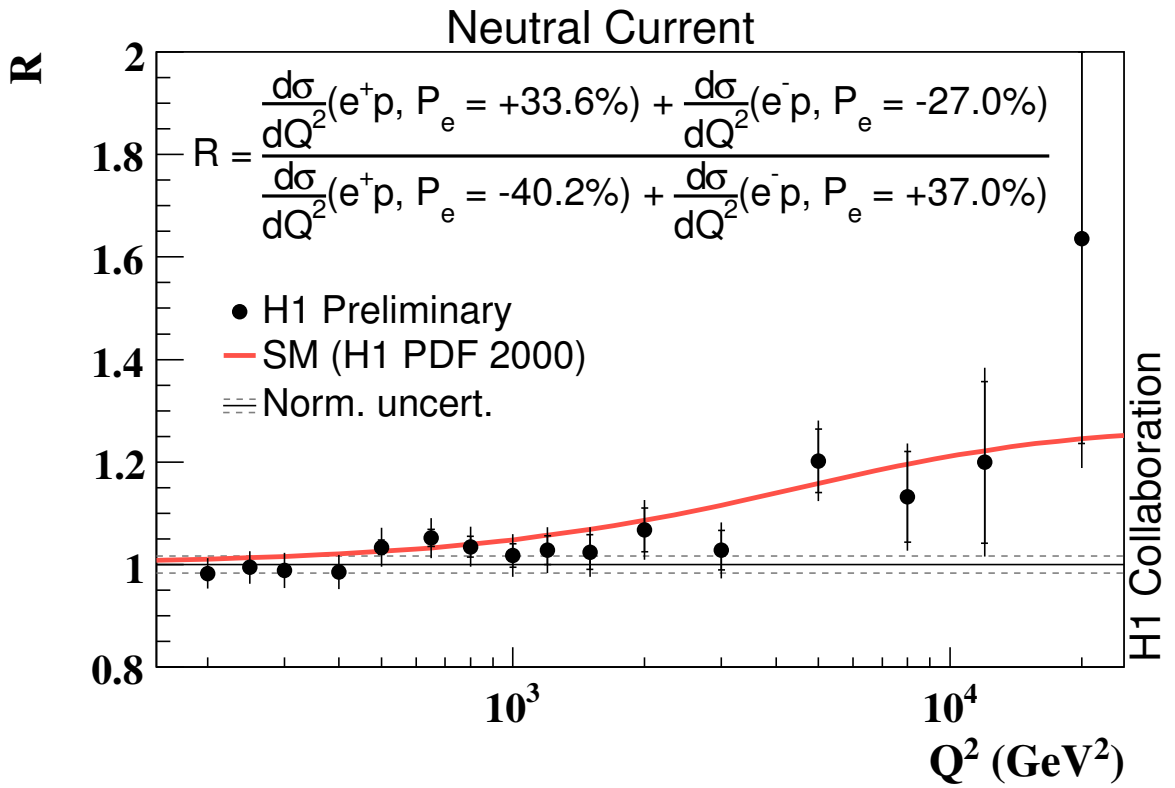

Figure 6: The Q^2 dependence of the combined $e^{\pm}p$ L and R NC cross section ratio R. The data (solid points) are compared to the Standard Model prediction. The inner error bars represent the statistical uncertainties and the outer error bars represent the total errors. The normalisation uncertainty is not included in the error bars.

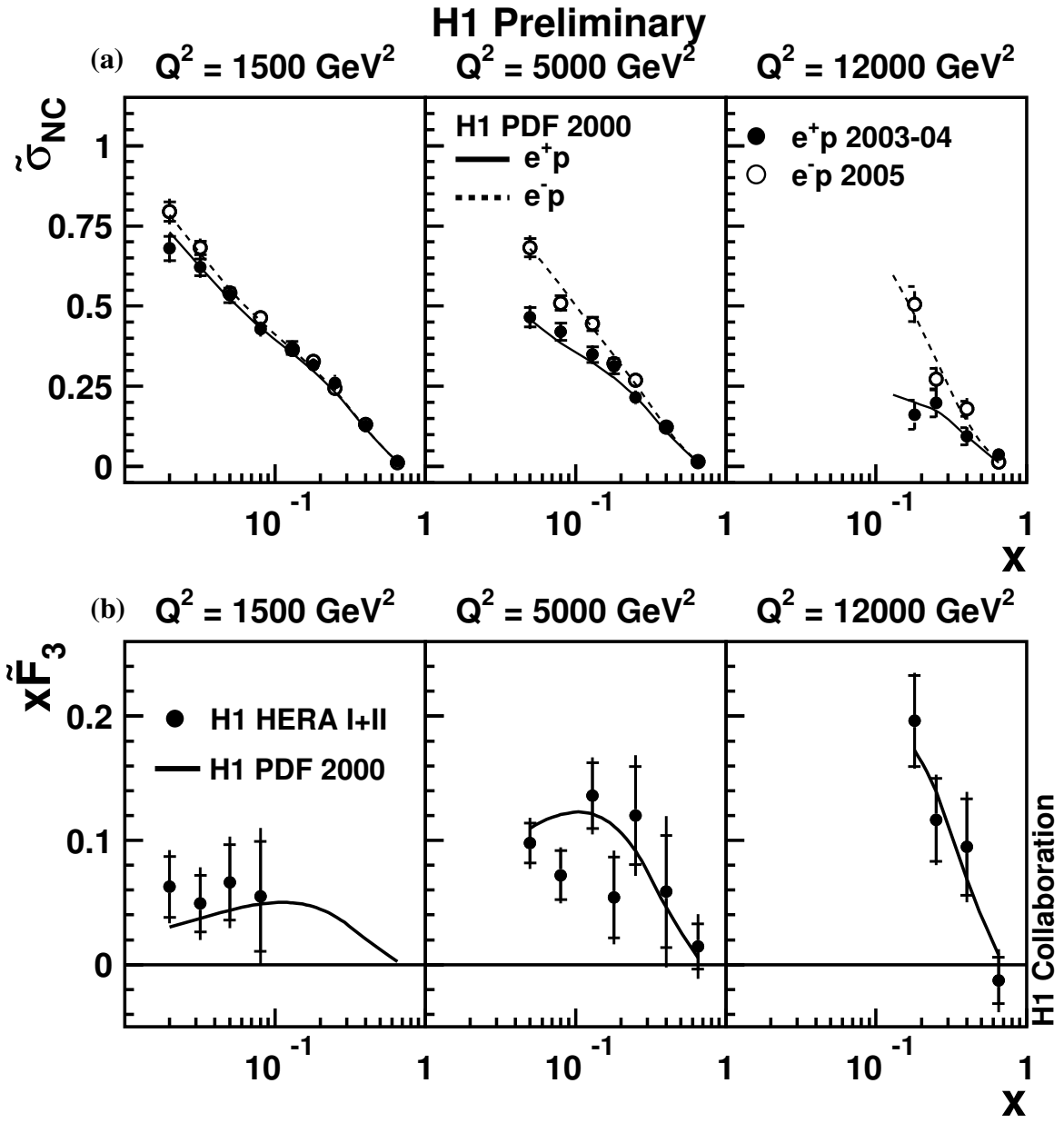

Figure 7: The unpolarised reduced cross sections $\tilde{\sigma}^{\pm}(x, Q^2)$ are shown in (a) for HERA-II data (open/solid points) compared to the Standard Model (solid/dashed curves). The structure function $x\tilde{F}_3$ evaluated using HERA-I and HERA-II data is shown in (b) (solid points) compared to the Standard Model (solid curve). The inner error bars represent the statistical uncertainties and the outer error bars represent the total errors. The normalisation uncertainty is included in the error bars for (b) only.

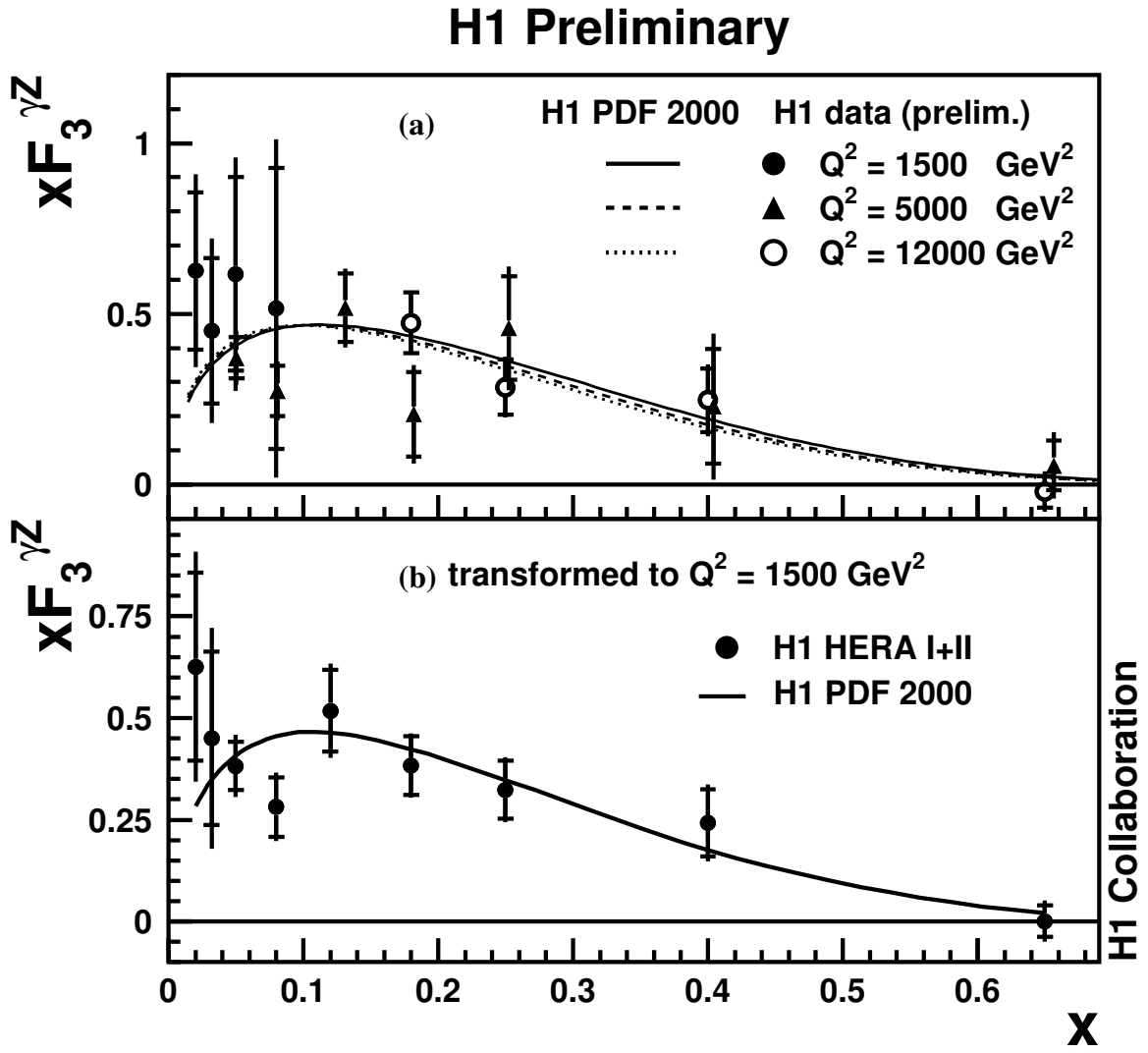

Figure 8: The structure function $xF_3^{\gamma Z}$ extracted from all HERA-I and HERA-II data (solid and open points) is shown in (a) for three Q^2 bins together with the Standard Model expectation (full, dashed and dotted curves). In (b) the data are transformed to $Q^2 = 1\,500$ GeV^2 and combined in each x bin. The inner error bars represent the statistical uncertainties and the outer error bars represent the total errors. The normalisation uncertainty is included in the error bars.